# Temperature-Dependent Properties of ALD-Grown $TiO_2$ Thin Films

Nimarta Kaur Chowdhary, and Theodosia Gougousi*

Department of Physics

University of Maryland, Baltimore County (UMBC), Baltimore, MD 21250, USA

*Corresponding author email: gougousi@umbc.edu

## Abstract:

This study investigates the presence of titanium oxynitride bonds in $TiO_2$ thin films grown by Atomic Layer Deposition using tetrakis dimethyl amino titanium and water at temperatures between 150°C – 350°C and its effect on the films' optical and electrical properties. Compositional analysis using X-ray photoelectron spectroscopy reveals increased incorporation of oxynitride bonds as the process temperature increases. Furthermore, depth profile data demonstrates an increase in the abundance of this type of bonding from the surface to the bulk of the films. Ultraviolet-visible spectroscopy measurements correlate increased visible light absorption for the films with elevated oxynitride incorporation. The optical constants (n, k) of the films show a pronounced dependence on the process temperature that is mirrored in the film conductivity. The detection of oxynitride bonding suggests a secondary reaction pathway in this well-established ALD process chemistry, that may impact film properties. These findings indicate that the choice of process chemistry and conditions can be used to optimize film properties for optoelectronic applications.

## Keywords:

Atomic Layer Deposition, Titanium Oxide, Titanium Oxynitride, Secondary reaction pathways, optical properties, electrical properties

## Introduction:

Transition metal oxides (TMOs) are typically regarded in the literature for having high refractive indices, being wide-bandgap semiconductor materials, and being transparent or semi-transparent in the visible range. Due to their low cost, high abundance, eco-friendliness, and low-toxicity [1,2] there has been an increased interest in using and modifying these materials for visible light applications. Of these various TMO materials, titanium dioxide ($TiO_2$) is well-known as an effective photocatalyst for industrial and environmental applications, such as water and air purification [3,4]. In its pure state, however, it is mostly active under UV-light irradiation[5]. Appropriate modification of the composition of pure $TiO_2$ may enhance the catalytic properties in the visible and extend the existing range of applications.

The materials' optical, electronic, and catalytic properties can depend on the surface morphology, crystalline phase, and composition [6,7]. Common approaches towards modifying $TiO_2$ include coating the surface with noble metal nanoparticles [8,9], intentional doping [6,10,11], and altering the crystal structure [12,13]. Of the various methods to deposit titanium-based oxides, atomic layer deposition (ALD) is routinely used for thin film growth. Metal-organic precursors commonly used in the ALD process include titanium tetrachloride ($TiCl_4$)[14], titanium isopropoxide (TTIP) ($Ti[OCH(CH_3)_2]_4$)[15], and tetrakis(dimethyl amino) titanium (IV) (TDMAT) ($Ti[N(CH_3)_2]_4$)[16], typically in combination with $H_2O$ or $O_2$ as the oxidants.

TDMAT offers significant advantages among these precursors due to its non-toxic and non-corrosive nature, both in the precursor itself and its by-products .

Previous work demonstrates that some amorphous ALD $TiO_2$ films grown using TDMAT and $H_2O$ exhibit a large nonlinear refractive index ($n_2$) [17]. It was hypothesized that impurities in the form of oxynitride bonds incorporated during the ALD deposition process were responsible for the observed nonlinear optical response. Although TDMAT is routinely used for ALD depositions of $TiO_2$ films, investigations into the temperature-dependent compositional gradients within these films remain scarce.

While it is generally assumed that metal oxide films produced through ALD primarily consist of the target material, with only minor contributions from carbon-containing species, our study reveals that the choice of process conditions, particularly the deposition temperature, can significantly impact the composition and as a result, the optical and electrical properties of the films. More specifically, this work addresses that gap by systematically analyzing the evolution of compositional gradients and their effect on the thin film properties. By varying growth parameters, such as the deposition temperature and purge time, we explore modifications to the film composition and the resulting optical and electronic properties. Attention is also given to the high-temperature regime where thermal decomposition and rapid desorption mechanisms dominate[18]. The effect of the process conditions on compositional variations and their correlation with film properties must be carefully considered in the design and optimization of applications relying on these films.

## Experimental Methods:

### *Sample Preparation*

ALD is the main technique used to grow $TiO_2$ films in this work. Control $TiO_2$ films are deposited using Physical vapor deposition (PVD). All films are grown on double polished Si (<100>, P-type, Boron-doped, 10-20 $\Omega \cdot$cm), and fused quartz microscope slides. The silicon-based substrates are cleaved into assorted sizes and the quartz substrates are cut from larger quartz microscope slides (76.2 x25.4x1mm) to approximately 20mm by 25.4mm pieces. Silicon substrates are cleaned in acetone, methanol, and deionized (DI) $H_2O$ for 5 minutes each. Quartz substrates are cleaned in methanol and isopropanol for 10 minutes each and rinsed in DI $H_2O$ for 5 minutes. Both substrates are dried with $N_2$. The samples deposited on the quartz were used for Ultraviolet-visible (UV-Vis) and Spectroscopic Ellipsometry (SE) measurements and the samples deposited on Si were used for all the other standard characterization techniques.

Control $TiO_2$ films are grown using nonreactive radio frequency (RF) magnetron sputtering in a Denton Vacuum DV-502A system using a $TiO_2$ target (99.9999% pure, 3”) with 15 sccm of argon gas. The substrates are mounted to a rotating chuck and are kept at room temperature during depositions. An Advanced Energy RFX 600 and ATX 600 RF Generator is used with this system. Plasma is ignited at a power of 70W, and the power is slowly increased to 145W over 10 minutes. The target is then cleaned with the shutter closed for 10 minutes before the deposition. The chamber pressure is held at ~ 6 x $10^{-3}$ Torr during the process. These samples are used as the reference and are labeled “PVD $TiO_2$” in this work.

ALD $TiO_2$ films are deposited using a custom-built stainless-steel hot-wall flow tube ALD reactor, as described by Hackley and Gougousi [19], and is modeled after the reactor designed by Ylilammi and Becker et al. [20] [21]. Films are deposited between 150°C – 350°C in 25°C increments at 5, 10, and 30s

purge times using tetrakis(dimethyl amino) titanium (IV) (TDMAT) ($Ti[N(CH_3)_2]_4$, 99.999%, Sigma-Aldrich) and DI $H_2O$ as the oxidizer. The fixed-volume method, described by Hausmann et al.[22], is used for the precursor delivery. The TDMAT bubbler is heated to 81°C and DI $H_2O$ is kept at room temperature. $N_2$ is used as the operating gas and the system is actively pumped with a rotary vane oil pump to maintain a pressure between 250 – 275 mTorr during the depositions. LabVIEW™ software from National Instruments (NI) manages the total number of cycles, dosage times, temperatures, and purge times for the deposition process. Quartz substrates are mounted on top of quartz sacrificial pieces to minimize backside deposition. Companion silicon pieces are placed next to the quartz samples to ensure consistency of the deposited film. A thickness of 50 nm was targeted for all film growth. The films were not subjected to any post-deposition treatment.

***Sample Composition and Transmission***

Thin film thickness is measured using standard lithography approaches, buffered oxide etch, and a KLA-Tencor Alpha-Step 500 Profilometer. X-ray photoelectron Spectroscopy (XPS) was used for compositional analysis. High-resolution elemental scans with a 0.1 eV step size in the Ti 2p, N 1s, C 1s, and O 1s regions were conducted using a Kratos AXIS ULTRA-DLD XPS instrument equipped with an Al Kα X-ray source (1486.6 eV) and a 165-mm electron energy hemispherical analyzer. Samples were analyzed as received without sputter surface cleaning. The spectra were calibrated to the C 1s adventitious carbon peak at 284.8 eV using CasaXPS software. The core-level spectra are analyzed and fit using Gaussian-Lorentzian line shapes in the product (GL 30) and sum form (SGL 40) and a Shirley background. For select samples, an Argon ion beam (4 keV) was used for depth profiling on 3 x 3 $mm^2$ of the sample's surface to determine some elemental profiles through the bulk of the film. Depths of 0, 2, 4, 10, and 30 nm were used. A 9-point smoothing was applied to the depth profile data using a 2nd-order Savitsky–Golay filter to reduce noise.

Additional information regarding sample composition through the layers was probed using time of flight secondary ion mass spectroscopy (ToF-SIMS). Positive high-mass resolution depth profiles were performed using a TOF-SIMS NCS instrument. The analysis field of view was 150 x 150 $\mu m^2$ ($Bi_3^+$, 30 keV, 0.3 pA) with a raster of 128 pixels by 128 pixels along the depth profile. The cycle time was fixed to 100 µs (m/z = 0 – 911 amu). All depth profiles were point-to-point normalized by the total ion intensity and the data was plotted using a 5-point adjacent averaging technique. Furthermore, a JASCO V-570 UV/VIS/NIR Spectrophotometer measured the absorbance in the 200 nm – 2500 nm wavelength range on the quartz films.

***Surface Morphology and Crystallinity***

The surface roughness of films deposited at different temperatures and purge times was evaluated using the MFP-3D Origin™ atomic force microscope (AFM). Root mean square (RMS) roughness values were extracted from the AFM images using the Gwyddion software package[23].

Fourier transform infrared spectroscopy (FTIR) was used in transmission mode using a Nicolet 4700 FTIR spectrometer to analyze film crystallinity. A DTGS polyethylene (PE) detector with a solid substrate beam splitter was used for the spectral range of 600–50 $cm^{-1}$ (far-IR). Data were collected and analyzed using the vendor-provided OMNIC software. Sample spectra were ratioed to a native oxide silicon substrate. Crystallinity was further confirmed using X-ray diffraction (XRD) with a C2 Advance diffractometer equipped with Bragg-Brentano geometry and Cu-Kα radiation (λ = 1.54 Å).

***Optical Constants and Conductivity***

The film thickness and the wavelength-dependent optical functions, such as the refractive index, n, and extinction coefficient, k were simultaneously determined using a fixed angle (70°) Woollam alpha-SE Ellipsometer. For transparent thin films, where absorption is negligible in the visible (k = 0), single-angle SE measurements (ψ, Δ) are adequate for obtaining the thickness and wavelength-dependent n on silicon substrates. For absorbing thin films, where k is non-zero in the visible, quartz substrates are used for obtaining the optical functions. Intensity-based wavelength-dependent transmission (T) measurements at 90° supplement the single angle SE measurements (ψ, Δ) at 70°, a method known as SE + T[24,25]. To mitigate backside reflections from the quartz substrate, Magic Scotch Tape® with a cloudy finish is applied to the back of the quartz substrate before the SE measurements are taken[26]. At the standard acquisition rate, measurements are taken in the 380 – 900 nm wavelength range (1.4 eV – 3.3eV).

Post-measurement analysis uses optical modeling to extract the thickness and optical functions. The "Glass with Transparent Film" model built-in to the CompleteEASE® software from Woollam[27] is used for transparent films using the 7059_Cauchy substrate with a Cauchy dispersion model[28]. For absorbing films, SE and T measurements are analyzed simultaneously using the "Glass with Absorbing Film (with backside reflection)" model, which can account for some minimal backside coating. A 7059_Cauchy material of 1 mm thickness is used for the fused silica substrate and a B-Spline layer for the absorbing film[29]. The starting material is $TiO_2$, the resolution is set to 0.1 eV, and the angle offset and surface roughness are turned off. Additionally, a SIGNATONE Pro4 4-point probe head with a Keithley 2400 SourceMeter measured thin film resistivity on the silicon-based substrates with a fixed current of 1 mA.

## Results & Discussion:

For most ALD processes, an optimal range of process temperatures is identified as the "ALD window." Films grown outside of the "ALD Window" may have non-ideal type deposition effects such as poor growth rates, nonuniformities, and impurities within the bulk of the films [30]. Purge time is another

**Table 1:** Summary of ALD $TiO_2$ film thickness on silicon substrates

| Deposition Temperature (°C) | Profilometer Thickness (nm) | | |
|---|---|---|---|
| | 5s purge | 10s purge | 30s purge |
| 150 | 55 ± 4 | 55 ± 3 | 56 ± 3 |
| 175 | 64 ± 5 | 51 ± 3 | 54 ± 3 |
| 200 | 55 ± 3 | 56 ± 3 | 57 ± 4 |
| 225 | 48 ± 3 | 54 ± 3 | 52 ± 3 |
| 250 | 56 ± 4 | 59 ± 5 | 55 ± 4 |
| 275 | 43 ± 3 | 53 ± 5 | 48 ± 4 |
| 300 | 47 ± 4 | 50 ± 3 | 40 ± 5 |
| 325 | 36 ± 4 | 38 ± 3 | 46 ± 3 |
| 350 | 52 ± 3 | 55 ± 3 | 50 ± 4 |

Deposition Temperature (°C)
Profilometer Thickness (nm)
5s purge
10s purge
30s purge
150 55 ± 4 55 ± 3 56 ± 3
175 64 ± 5 51 ± 3 54 ± 3
200 55 ± 3 56 ± 3 57 ± 4
225 48 ± 3 54 ± 3 52 ± 3
250 56 ± 4 59 ± 5 55 ± 4
275 43 ± 3 53 ± 5 48 ± 4
300 47 ± 4 50 ± 3 40 ± 5

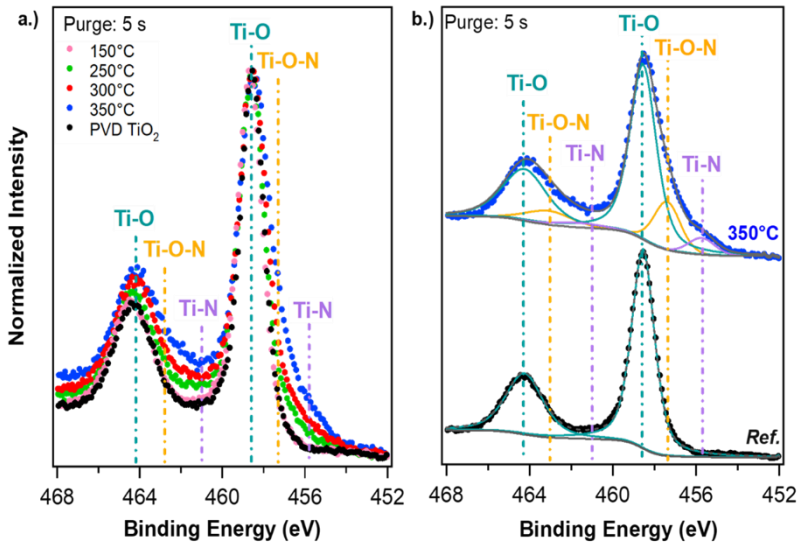


**Fig. 1:** a) High-resolution, normalized, and overlayed Ti 2p XP Spectra data for 5s purge ALD films. The spectra for the PVD $TiO_2$ reference sample are shown in black. b.) Sample fits (colored solid lines) for the 350°C, 5s ALD, and PVD $TiO_2$ samples.

important parameter used to ensure the separation of the two precursor pulses. If purge times are too short, residual by-products and unreacted precursors may remain, leading to a quasi-chemical vapor deposition (CVD) process that changes the overall composition and properties[31].

These two parameters, temperature and purge time, were used in this work to influence the film composition. A target thickness of 50 nm was used for all growth conditions to minimize its influence on the optical measurements. For this reactor, the minimum growth per cycle (GPC) across all purge times occurs at 200°C, with growth values of approximately 0.05 nm/cycle. The measured thickness for all ALD films used in this work is shown in Table 1. The thickness of the PVD $TiO_2$ film is measured to be 54 ± 5 nm.

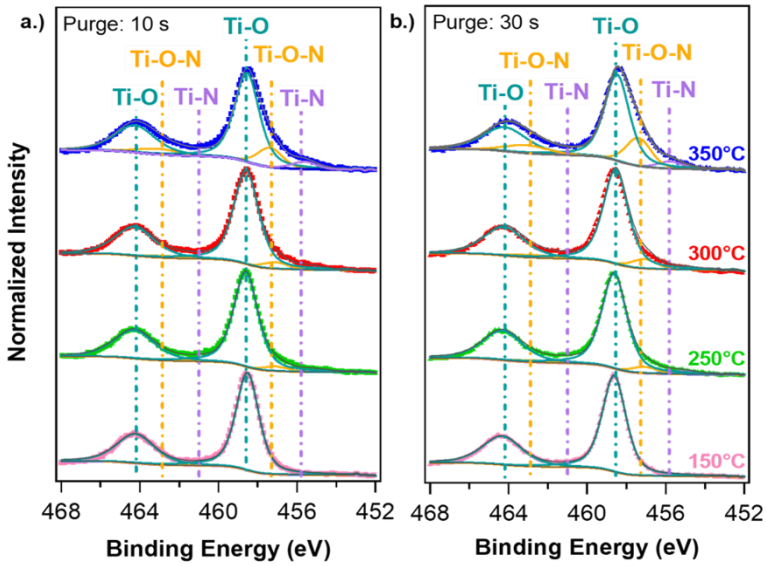


**Fig. 2:** High-resolution, normalized, and overlayed Ti 2p XP spectra ALD films deposited with a.) 10s purge b.) 30s purge times.

***Film Composition***

XPS was used to analyze the film composition, with high-resolution scans of the Ti 2p region shown in Fig. 1 for some as-deposited ALD films with a 5s purge time and the reference PVD $TiO_2$ film. When the spectra are overlayed and normalized (Fig. 1a), low binding energy (BE) features between ~455 – 457 eV in the Ti 2p spectra appear in the ALD films as the process temperature increases. These features are absent in the reference $TiO_2$ films. To illustrate this clearly, Fig. 1b shows the fits for the reference PVD $TiO_2$ film (black) and the ALD film deposited at the highest temperature examined, 350°C (blue). The PVD $TiO_2$ film exhibits the expected Ti $2p_{3/2}$ peak at ~458.5 eV and the Ti $2p_{1/2}$ peak at ~464.3 eV [32], labeled Ti-O, referring to the oxide component in $TiO_2$.

The Ti 2p spectral deconvolution shows additional features for the 350°C ALD film. A secondary peak at ~456 eV is attributed to titanium nitride (TiN) bonding within the $TiO_2$ matrix [33] and is labeled Ti-N. The peak at ~457 eV is associated with titanium oxynitride ($TiO_xN_y$)[10,33] and is labeled Ti-O-N. When similar XPS measurements and analysis are conducted for the 10s and 30s purge ALD films, the behavior in the Ti 2p region (Fig. 2) is similar to the 5s purge films; the low-intensity BE peaks increase as the process temperature increases. While different peak assignments are possible for the features observed in the Ti 2p region, complementary information from another spectral region could provide a definitive assignment.

In the N 1s region, shown in Figure 3, intensity data (counts per second) is plotted as a function of BE for select as-deposited ALD films and the reference $TiO_2$ film. The spectra for the ALD films deposited below 250°C show no significant spectral features, except for a broad peak at ~400 eV. As the ALD process temperature is raised above 250°C, new spectral features between ~395 – 398 eV emerge and become more pronounced with increasing temperature. These features are most prominent for the films deposited at 350°C and sample fits for these films are shown in Fig. 3 for all purge times.

The spectral deconvolution is accomplished using three peaks with BE in the ~396 – 400 eV range. The high BE feature at ~400 eV, labeled $N_S$, is present in both ALD and PVD films. This peak can be attributed

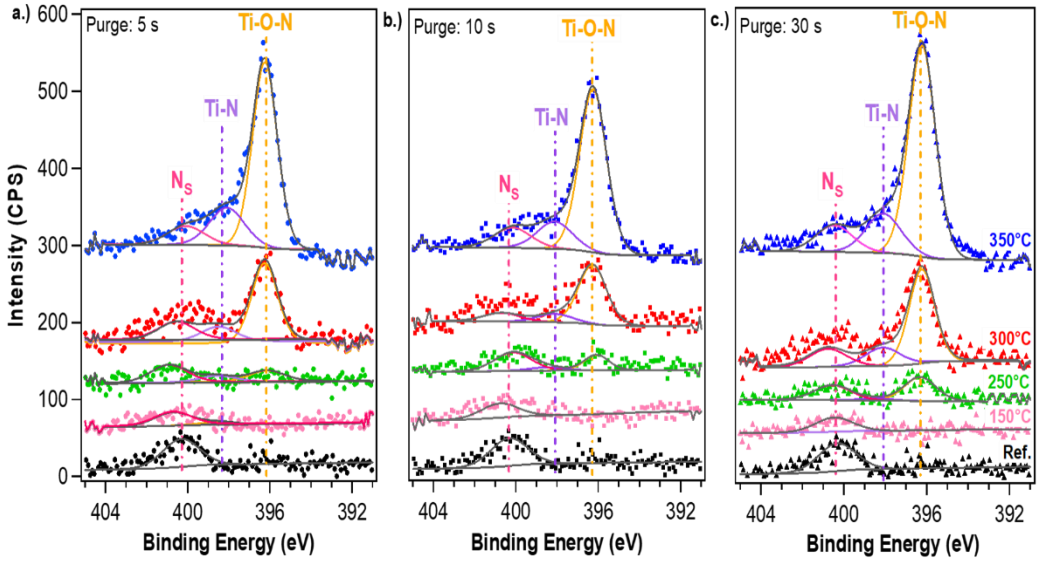


**Fig. 3:** High-resolution N 1s XP Spectra and sample fit (colored solid lines) for select ALD films deposited using a.) 5s purge times b.) 10s purge times c.) 30s purge times. The PVD $TiO_2$ reference sample is shown in black.

to the presence of amine precursor ligands[34] or nitrogen-containing contaminant surface species[35]. The remaining two peaks have been correlated to the presence of Ti-N/Ti-O-N bonds[36]. In general, the higher BE peak at ~397 – 398 eV is assigned to Ti-N[37] while the lower BE peak at ~396 eV is assigned to $TiO_xN_y$, though the exact location varies somewhat depending on the chemical environment and oxynitride stoichiometry[38]. We follow these guidelines for assigning the observed peaks at ~396 eV and ~397 eV in the spectra to Ti-O-N and Ti-N, respectively. Peak assignments between the Ti 2p and N 1s regions are consistent and in good agreement across all purge times; both indicate traces of Ti-N and increasing concentration of Ti-O-N bonding as the process temperature increases.

XPS was used to extract compositions[39] for all samples and the atomic percentage (at.%) of bonded nitrogen and carbon as a function of process temperature is shown in Figure 4. The bonded nitrogen contained in the ALD films ranges from ~ 0 – 5.4 at.% and generally increases monotonically as a function of the process temperature [16,40]. Variation is also seen in the at.% of bonded carbon, with values ranging from ~2.1 – 7.6 at.%. The variation is not monotonic, reaching a minimum at 275°C and increasing after that by approximately 2 – 3 at.%. For the PVD $TiO_2$ film, we find 0 at.% bonded N and ~3.9 at.% bonded carbon.

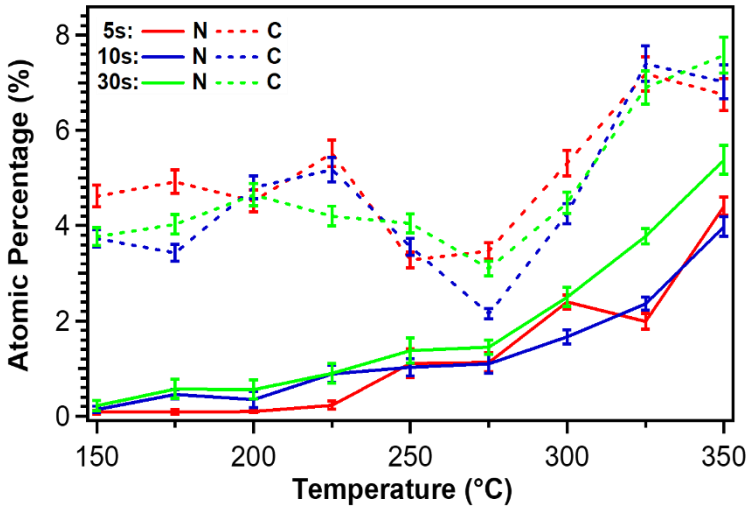


**Fig. 4:** Atomic percentage (at.%) of bonded nitrogen (solid lines) and bonded carbon (dashed lines) as a function of temperature for 5s (red), 10s (blue), and 30s (green) purge time for ALD $TiO_2$ films. Results are only for the as-received sampling depth and may differ from the bulk composition.

Since the compositional analysis does not demonstrate the presence of substantial Ti-O-N/Ti-N bonding for some films below ~225°C, depth profiling in the N 1s region was performed on select films (150°C, 200°C, 350°C and 5s purge) to investigate the presence of such bonding in the bulk and the results are presented in Figure 5. For the 150°C film (Fig. 5a) the absence of any significant nitrogen is confirmed from a depth of 2 nm to the bulk (30 nm). The small feature at ~400 eV is observed only at the surface scan, confirming its assignment as a nitrogen-containing surface contamination species. As the ALD deposition temperature increases to 200°C (Fig. 5b), no features are initially detected on the surface. At a depth of 4 nm, a small Ti-O-N/Ti-N feature at ~397 eV appears, intensifies between 4 – 10 nm, and remains unchanged between 10 – 30 nm. At the highest temperature used in this work, 350°C (Fig. 5c),

oxynitride species are detected at the surface, demonstrated by the large peak at ~397 eV. The intensity of this peak increases between 0 – 10 nm and then stabilizes between 10 – 30 nm.

These depth profile results indicate that the films deposited at 150°C are the purest when considering oxynitride-based impurities, as the nitrogen concentration remains relatively unchanged from surface to bulk. In contrast, films deposited at higher temperatures contain nitrogen-based impurities, with their concentration increasing in the bulk of the film. TiN is known to oxidize upon ambient exposure[17,41] and the depth profiling confirms this by detecting an increasing concentration of titanium oxynitride as we probe deeper from the film surface.

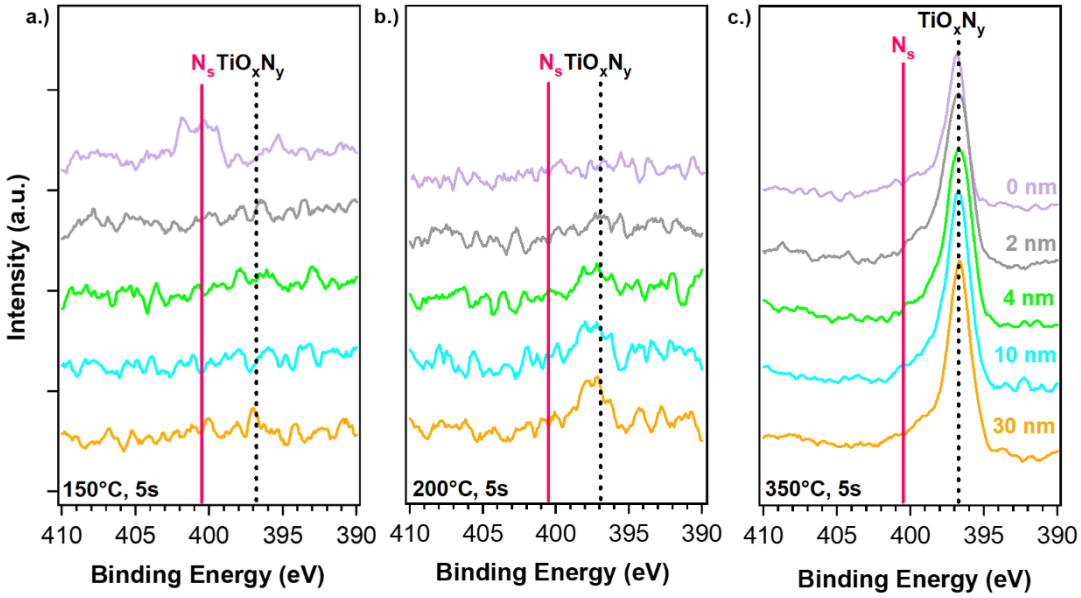


**Fig. 5:** High-resolution N 1s XP depth profile results for films deposited using 5s purge at a.) 150°C b.) 200°C and c.) 350°C. A depth of 0 nm refers to the surface. The solid pink line at ~ 400 eV and dotted black line at ~397 eV are used to track nitrogen-containing species through the bulk of the film.

ToF-SIMS was used to analyze the presence and distribution of oxynitride species for a subset of ALD $TiO_2$ films. The signals of interest correspond to mass/charge ratios of 62 and 64. The analysis of these signals needs to consider isotope effects. Titanium has five isotopes with a substantial abundance. Of these, the ones of interest are $^{46}Ti$ (8.25%), $^{48}Ti$ (73.7%), and $^{50}Ti$ (5.18%). The signal at 62 amu, has contributions from both $^{48}Ti^{14}N$ and $^{46}Ti^{16}O$ and the signal at 64 amu has contributions from both $^{50}Ti^{14}N$ and $^{48}Ti^{16}O$. If we assume the natural abundance of the titanium isotopes in the TDMAT precursor, then the expected ratio of the signal for mass 62 to mass 64 should be 0.112 for a pure $TiO_2$ film. A higher ratio can then be interpreted as the presence of Ti-N bonding in the film. Figure 6 shows the mass 62/mass 64 ratio as a function of depth from 1 to 30 nm for three ALD films. A depth of 0 nm was excluded due to surface effects.

For the film deposited at 200°C, an average ratio close to the expected value for pure $TiO_2$ is obtained. More specifically, from 1 – 4 nm, the average value is 0.112 ± 0.001, indicating only minimal traces of nitrogen. Beyond 4 nm, the average ratio increases slightly to 0.113 ± 0.002, indicating a minor increase in nitrogen concentration. These ToF-SIMS data follow the same trend as the 200°C XPS depth profile

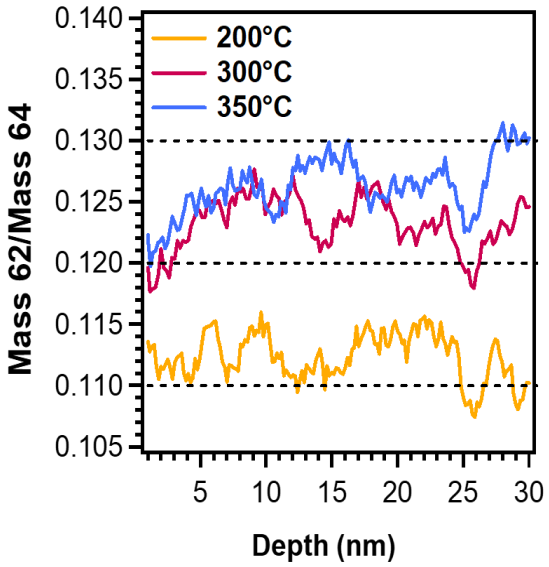


**Fig. 6:** ToF-SIMS results for select ALD films. This compares data from the signal at mass 62 and 64. Dashed black lines are plotted as guides for the eye.

results (Fig. 5b). The two films deposited at higher temperatures show a substantially higher value for the mass 62/mass 64 ratio. Additionally, the ratio increases as we move away from the film surface. For the 300°C film, the ratio increases from 0.118 to 0.128 from 1 – 9 nm and then averages to 0.123 ± 0.002 between 10 to 30 nm. For the film deposited at 350°C, a gradual increase from 0.120 to 0.130 is generally observed from 1 – 15 nm and then averages to 0.127 ± 0.002 between 16 to 30 nm.

These results are compatible with the XPS results that show an increase in the film's bonded nitrogen content with the process temperature. Overall, the ToF-SIMS data analysis and XPS depth profile analysis both lead to the same conclusion: the composition of the films at the film surface differs from that of the bulk, with some oxynitride found deeper or in increased abundance.

***UV-Vis Transmission***

UV-Vis spectroscopy was used to measure the absorbance of the ALD $TiO_2$ films on quartz substrates. The corresponding transmittance data are shown in Figure 7 for select deposition temperatures and purge times. For comparison, reference spectra for the PVD $TiO_2$ film with a similar thickness (~54 nm) and bare quartz substrates are included.

For the film deposited at 150°C with the 5s purge time (Fig. 7a, pink curve), the transmittance curve closely matches the reference $TiO_2$ film (black curve). At 633 nm, both show a transmittance of 72 %T. XPS depth profile results (Fig. 5a) confirm the absence of oxynitrides throughout the bulk of this film. However, at 200°C (light blue curve), the transmittance of the film deposited with a 5s purge decreases to 66 %T at 633 nm. The transmittance through the film can be influenced by both thickness and optical properties. Since the film thicknesses are similar, the decrease in transmittance at 200°C is attributed to oxynitride impurities[4,42]. This is supported by the N 1s depth profile (Fig. 5b). As the deposition temperature further increases, the transmittance at 633 nm decreases significantly: reaching 47 %T at 250°C (green curve) and 32 %T at 300°C (red curve). Minimal changes in transmittance occur between 300°C – 350°C, with a similar value of 33 %T at 350°C (blue curve).

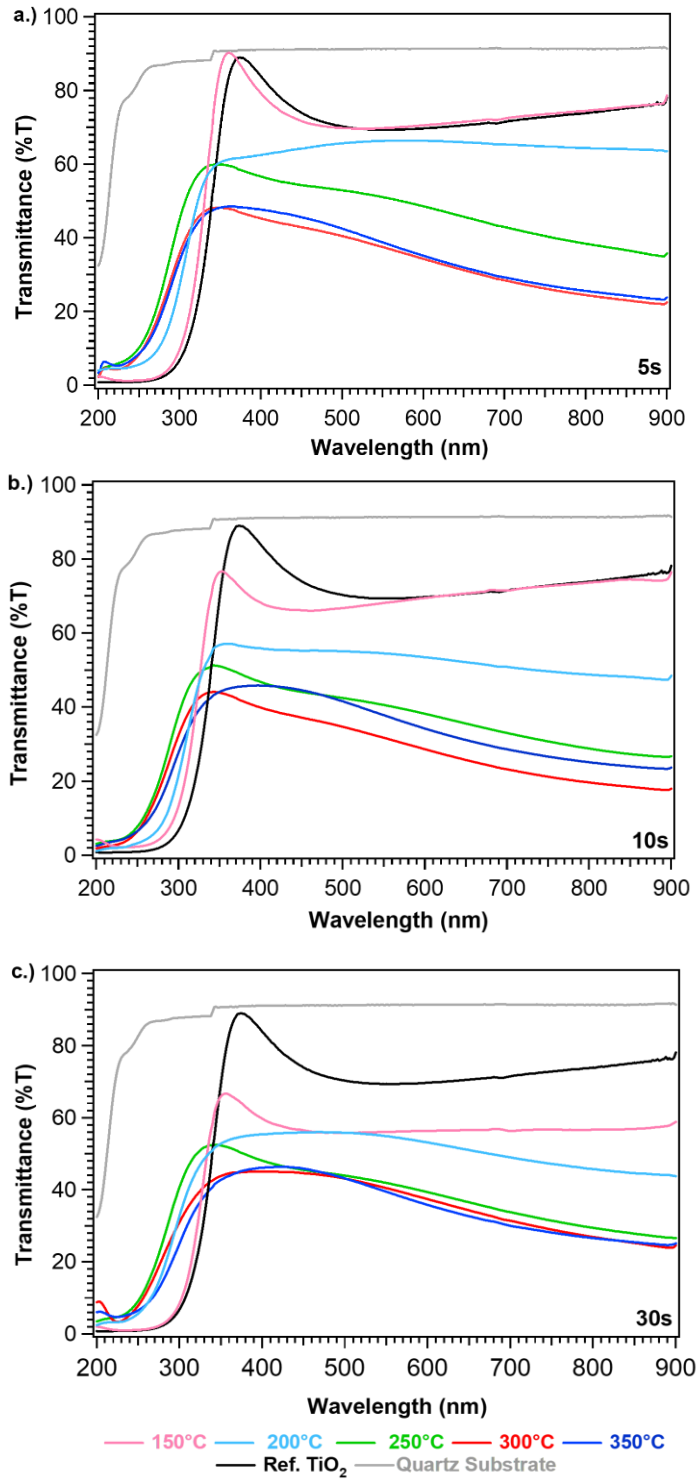


**Fig 7:** UV-Vis transmittance (%T) data for ALD $TiO_2$ films deposited at a.) 5s purge time b.) 10s purge time c.) 30s purge time. Reference $TiO_2$ and quartz substrate are shown in black and grey.

Similar trends are observed as the purge time increases to 10 and 30s. At 150°C, the 10s purge film (Fig. 7b) has a transmittance of 72%T, comparable to the reference $TiO_2$ film. The 30s film shows a lower measured transmittance of 62 %T at 633 nm (Fig. 7c), which is attributed to compositional differences as previous work on similar films with the 30s purge time[17] shows a trace presence of oxynitrides in the N 1s depth profile. As the deposition temperature increases, the transmittance at 633 nm for the 10s purge films decreases to 53 %T at 200°C, 39 %T at 250°C, 29 %T at 300°C, and 36 %T at 350°C. The lowest transmittance for the 10s films is observed at 300°C, while values at 250°C and 350°C are more similar. For the 30s films, transmittance values of 55 %T, 38 %T, 36 %T, and 34 %T are measured at the same temperatures, with minimal variation in the transmittance observed between 250°C– 350°C.

The UV-Vis results generally indicate a decreasing transmittance with increasing ALD deposition temperature for all purge times from ~200°C up to ~300°C which is again correlated with the increased oxynitride incorporation.

***Surface Morphology***

The surface of the as-deposited samples was examined with AFM and the results for both endpoint temperatures (150°C and 350°C) for all purge times are shown in Figure 8.

The films deposited at 150°C are smoother than the ones deposited at 350°C but in all cases, the RMS roughness ranges from 1 to 3% of the film thickness, which is typical for a well-behaved ALD process [22]. For both temperatures, the film RMS roughness improves with increased purge time as surface species are afforded more time for diffusion.

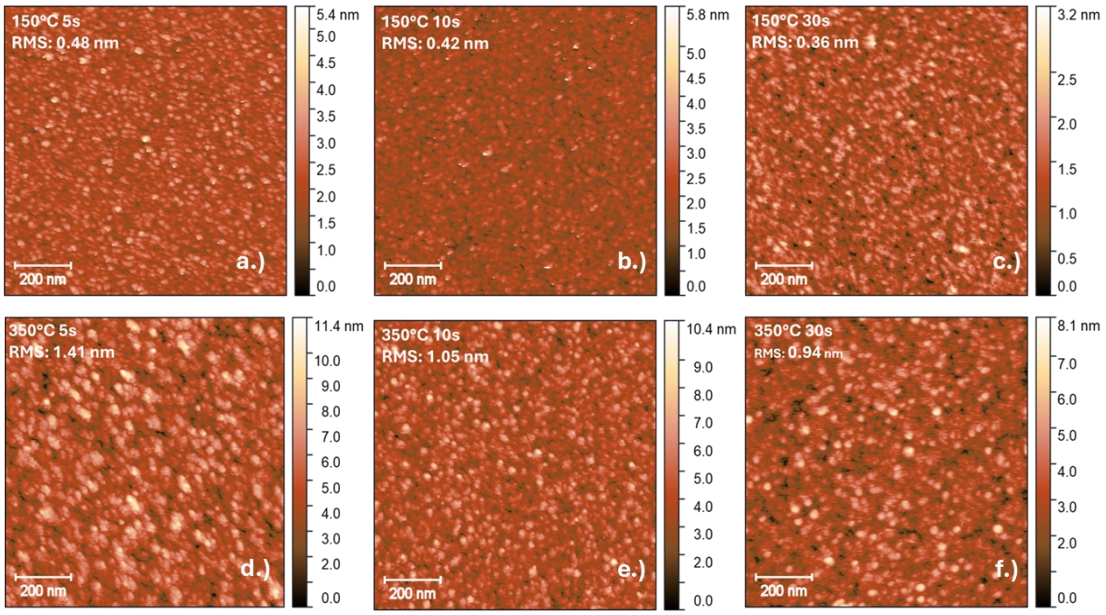


**Fig. 8:** 1 × 1 µm$^2$ AFM images of as-deposited films at 150°C (top) with a.) 5s purge b.) 10s purge c.) 30s purge and 350°C (bottom) with d.) 5s purge e.) 10s purge f.) 30s purge

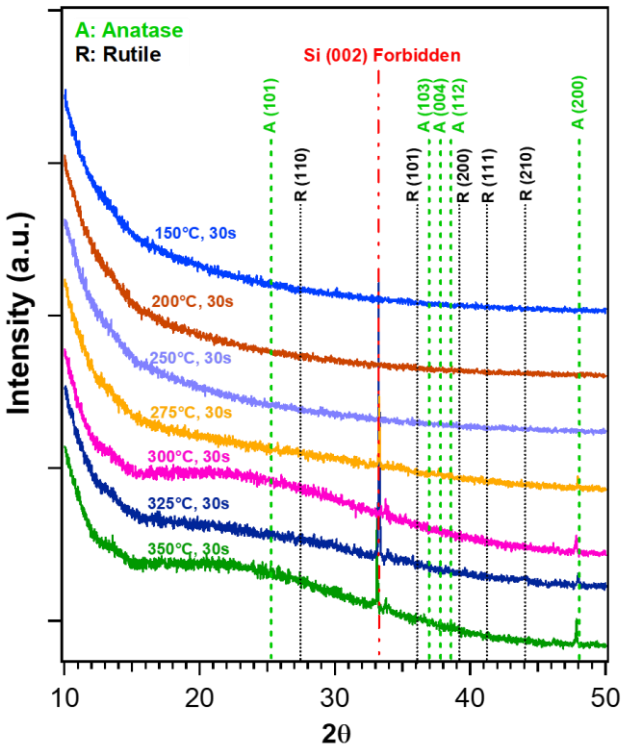


**Fig. 9:** XRD results for select ALD films deposited with a 30s purge time. JCPDS cards 21-1276 and 21-1272 are used to identify crystalline phases and families of planes.

***Crystallinity***

For all films in this work, the far IR portion of the spectrum (600 – 50 $cm^{-1}$) was used to study the textural evolution. Results are shown in Figure S1 for select deposition temperatures of 150°C, 250°C, and 350°C for all purge times. The as-deposited films are mainly amorphous, as demonstrated by the lack of distinct and sharp peaks from the $TiO_2$ phonon modes in their far-IR spectra (Figure S1).

The structural characterization of the films, initially assessed from their far-IR spectra, was confirmed using XRD measurements on select samples, as shown in Fig. 9. The XRD patterns predominantly display a broad background, indicative of an amorphous structure. Below 275°C, no sharp diffraction peaks are observed, confirming the absence of detectable crystallites. At 275°C and above, a low-intensity peak at 2θ = 48°, potentially corresponding to the (200) orientation of the anatase phase of $TiO_2$, emerges [43], with its intensity increasing slightly at higher deposition temperatures. The absence of other high-intensity rutile or anatase peaks suggests that the films remain primarily amorphous.

***Optical Constants***

The ALD films' optical functions (n, k) are obtained using the SE + T method[24,25]. As demonstrated in the XPS and ToF-SIMS depth profile analyses, the composition at the film surface can differ from the bulk composition, which is expected to influence the optical functions. To address this, a simple graded layer within the B-spline ellipsometer model[29] is used; the film is divided into five equal sublayers, each with its optical functions, to approximate the index gradient profile[27]. In this model, the refractive index (n)

varies linearly with depth, while the extinction coefficient (k) remains constant for all layers. Other grading types enable simultaneous variation of n and k with depth, but they include a greater number of fit parameters without a significant improvement in the goodness of fit and reliability of the extracted optical functions. For this reason, the simple grading model is chosen. The '% Inhomogeneity' fit parameter within the simple graded model is used to quantify the variation in n between the top and bottom layers of the film. The extracted k is an average over the bulk of the film. Surface roughness did not influence the optical functions (Fig. 8).

The SE + T method results in thickness measurements within ~5 – 8% of profilometer measurements on companion silicon samples (Table 1). The optical functions are obtained over the full wavelength spectrum for only the top and bottom layers (shown in supporting information Figure S2). In general, the top layers had increased n values compared to the bottom layers, in agreement with the measured dependence of the oxynitride concentration in the film bulk[44] (Figs. 5 and 6). For clarity, Figure 10a shows the range of n values from the top to bottom layers of the ALD films as a function of deposition temperature at the reference wavelength of 632.8 nm while Figure 10b shows the corresponding constant k value with an estimated error of 5% based on the goodness of fit. To aid the discussion, a range of values obtained from literature at this wavelength for $TiO_2$ [45] and TiN [46] thin films are plotted as bands in both figures. The reference PVD $TiO_2$ films have n = 2.4 and k = 0 at 632.8 nm, consistent with $TiO_2$.

For films deposited at or below 200°C, the optical model suggests $TiO_2$-like properties with minimal variation in the optical constants between the top and bottom layer, in agreement with the depth profile results. These films have only traces of oxynitride (Fig. 4) and their extracted refractive index falls within the expected range for typical $TiO_2$ films (Fig. 10a). In this temperature range, the extracted extinction coefficients (Fig. 10b) are consistent with previous reports for ALD $TiO_2$ films grown using TDMAT and $H_2O$[47,48]. At 150°C, films with 5 and 10s purge times show k values close to 0, whereas the 30s purge films have a higher k value due to the greater oxynitride incorporation[17]. At 200°C, all films show increased k values, but with distinct trends for each purge time: films with the 5s purge have the lowest k values, while those with the 10 and 30s purges show higher k values due to greater incorporation of nitrogen-containing species. These subtleties are reflected in the transmittance data (Fig. 7): films with the 5 and 10s purges have high transmittance at 150°C, giving the lower low k values, but at 200°C films with 10 and 30s purges have decreased transmittance, which results in higher k.

The increase in inhomogeneities (~15 – 35%) above 250°C suggests a more pronounced compositional gradient within the films, as indicated by the larger differences in n between the top and bottom layers (Fig. 10a). This finding agrees with the XPS and ToF-SIMS depth profile results that show a graded composition through the bulk. The films' optical constants (n, k) transition to TiN-like, in agreement with the increasing $TiO_xN_y$ content (Fig. 4). Considering the uncertainties, minimal variation in k is observed between 300 – 350°C for the 5s purge films while 10s purge films exhibit their greatest k at 300°C, within the uncertainty of the measurement. For the 30s purge films, only subtle variations are demonstrated in k between 275°C– 350°C. These limitations in k are exactly mirrored in the transmittance behaviors for each purge time and temperature (Fig. 7). A limiting-type behavior has also been observed in previous work of the measured nonlinear refractive index ($n_2$) values for the various ALD-$TiO_2$ films in the temperature range of 250°C – 300°C [17] with 30s purge times, in agreement with the trends observed here.

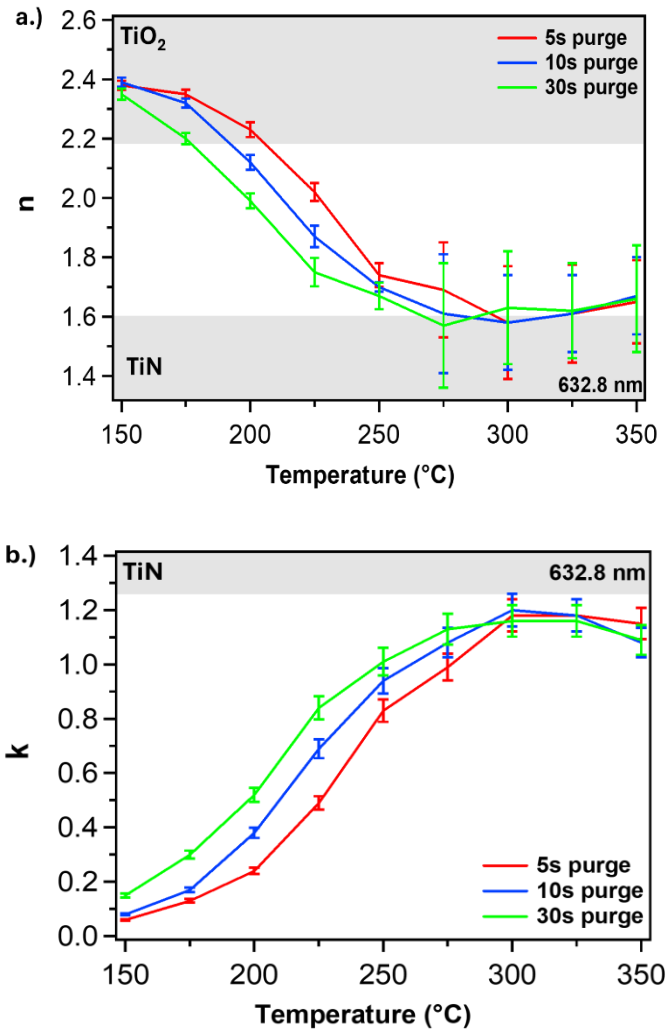


**Fig. 10:** a.) Refractive index (n) and b.) extinction coefficient (k) at 632.8 nm derived by SE + T for ALD films using 5, 10, and 30s purge times.

The variations in n and k provide a more detailed picture of how composition influences the optical properties. Overall, we find there is substantial variation in the film's optical constants from 200°C to 275°C, a temperature range that falls within the optimal ALD conditions reported in the literature[49].

***Conductivity***

While the optical constants provide information about the material's interaction with light, resistivity measurements offer a complementary view of the composition and electrical properties. We measured the room-temperature resistivity of PVD and ALD films across all deposition temperatures and purge times using a four-point probe. The resistivity measurements were converted to conductivity values, and are plotted in Figure 11 as a function of process temperature.

ALD films deposited at lower temperatures (150°C – 200°C) exhibit conductivities ranging from 550 to 1000 S/m. The conductivity of these films is about an order of magnitude higher than that measured for

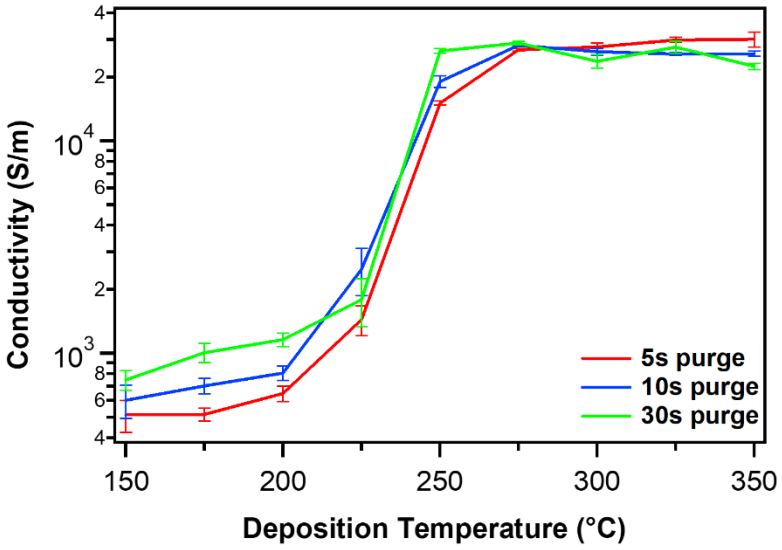


**Fig. 11:** Room temperature conductivity results for ALD films grown at 150°C – 350°C on silicon substrates.

the reference PVD films (111 ± 44 S/m). The films are mostly transparent at these temperatures (Fig. 7), but their conductivity is roughly one to three orders of magnitude lower than that typically observed for transparent conductive oxides (TCOs)[50,51].

As the deposition temperature increases to 250°C, the conductivity rises significantly, reaching values between 20,000 and 25,000 S/m – approximately two orders of magnitude higher than that of the reference PVD $TiO_2$ films. Little variation in conductivity is observed between 250°C – 350°C. While these conductivity values are comparable to or slightly lower than those of typical TCOs, the transparency of our films decreases considerably at higher temperatures (Fig. 7).

The values observed for the higher temperature films are on the order of $10^4$ S/m, which is well below the typical values of $10^5$ - $10^7$ S/m for TiN thin films[52], but still significantly higher than that obtained for the reference PVD sample. The deviation of the measured conductivity from the reference $TiO_2$, and the dependence of the conductivity on the process temperature are similar to the behaviors observed in the transmittance data (Fig.7) and the optical constants (Fig. 10). These properties can be attributed to the increased incorporation of oxynitride and carbon bonding in the film[53], which is confirmed by XPS and ToF-SIMS. This significant change in conductivity between 200°C and 250°C is particularly critical, as both temperatures fall within the process's "ALD window". As a result, the choice of process temperature within this range can have a significant impact on the insulating properties of the resulting film.

***Effect of Temperature and Purge Times on Film Composition***

The process chemistry based on the reaction of alkyl amine precursors with water used in this work has been widely used for the formation of a variety of transition metal oxide films. During a typical four-step ALD deposition cycle, the surface reactions for the ideal ligand exchange[54] between TDMAT and $H_2O$ are described as follows:

TDMAT half cycle

$Ti(NMe_2)_4 + \text{-OH*} \rightarrow \text{-O-}Ti(NMe_2)_3\text{*} + Me_2NH$ (Eqn. 1)

Here, (*) represents surface species, and "Me" refers to methyl groups ($CH_3$). In this step, the surface hydroxyl groups (-OH*) are replaced by dimethylamino ligands ($NMe_2$), producing dimethylamine ($Me_2NH$) as a by-product, which is removed by the $N_2$ purge.

$H_2O$ half cycle

$\text{-O-}Ti(NMe_2)_3\text{*} + 2H_2O \rightarrow TiO_2 - OH\text{*} + 3Me_2NH$ (Eqn. 2)

the remaining ligands are replaced by the hydroxyl groups, completing the deposition of the $TiO_2$ layer and preparing the surface for the next ALD cycle.

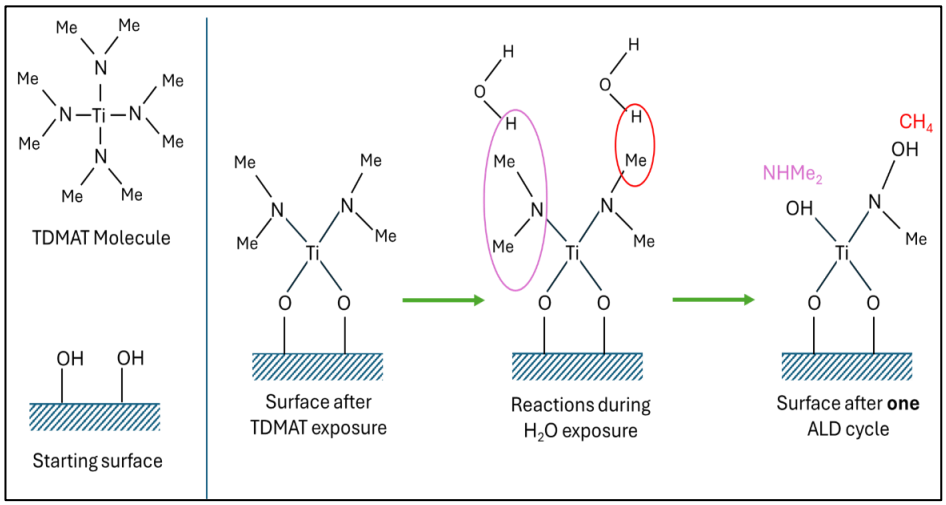


**Fig. 12:** Reaction mechanism for the formation of oxynitride species. The ideal exchange is shown in purple while the alternate pathway is shown in red.

However, as observed in other studies [55], the TDMAT/$H_2O$ ALD chemistry is not a simple ligand exchange process. Parallel and competing reaction pathways exist, even at relatively low temperatures. Precursor decomposition can even begin to occur at ~200°C[56], resulting in more complex film compositions. One possible reaction scheme that is consistent with the experimental observations is shown in Fig. 12.

The dominant reaction pathway is ligand exchange (shown in purple); dimethylamine is released as the primary by-product and the surface is returned to its original hydroxylated state. In an alternate reaction pathway (in red), partial ligand exchange may occur; a proton from the water may abstract one methyl ligand and form gas-phase methane ($CH_4$), leaving behind a hydroxyl group bonded to the nitrogen and possibly an unreacted methyl site. In subsequent precursor exposures, the hydroxyl-terminated nitrogen may act as a regular reaction site, potentially producing the oxynitride bonding detected in the films.

This proposed reaction scheme is compatible with experimental observations of $CH_4$ which have been attributed to direct TDMAT reactions, rather than successive decomposition of the dimethylamine reaction by-products[56]. Furthermore, it is compatible with observations of $TiN_xC_y$ surface species [49,54,56] and $CH_4$ by-products increase with process temperature due to the TDMAT decomposition [56].

Purge times only appear to significantly affect the film composition at the high-temperature range (> 275°C) – an increase in the purge time leads to higher bonded nitrogen content in the film. This indicates that precursor decomposition is partially responsible for the presence of these species. The bonded carbon content in the films increases with temperatures over 275°C, indicating that the process responsible for the formation of these species is thermally activated, but there is no significant purge time effect. Precursor decomposition and quasi-CVD are known to occur at these conditions, but the difference in the behavior of the nitrogen and carbon content with purge time suggests that there may exist more than one reaction pathway, such as precursor decomposition, and the partial ligand exchange reaction, as shown in Figure 12.

***Effect of Temperature and Purge Times on Film Properties***

Overall, we find that the process temperature and purge time can influence the resulting properties of the thin films differently in the various investigated temperature regions. In the lower temperature range (150°C – 200°C), the purge time has a more significant impact on optical constants and conductivity than the deposition temperature. In the mid-range (200°C – 275°C), both purge time and temperature influence these properties. However, neither parameter has a substantial effect in the high-temperature range (275°C – 350°C).

In the 150°C and 275°C range, carbon concentrations do not demonstrate a clear pattern while oxynitride concentrations generally increase with temperature, but can vary in amount for all purge times. At, and above, 200°C, decomposition products, and secondary reactions become increasingly important. We find that shorter purge times result in higher n, lower k, and lower conductivities. By reducing exposure to the reaction environment, shorter purge times decrease the chances for decomposition and secondary reactions which could otherwise lead to the formation of impurities that affect the optical constants and conductivity. Beyond 275°C, despite a general increase in carbon and oxynitride, variations between n, k, and conductivity become less pronounced. This may reflect more complete precursor decomposition or other high-temperature effects.

For example, other studies have shown that films deposited using TDMAT and $H_2O$ crystallize at deposition temperatures of 250°C and above [16]. Crystallite formation can alter structural order and visible light absorption, potentially increasing transmittance [45,57]. Additionally, Ryll et. al demonstrated that crystallite formation within an amorphous structure could decrease electrical conductivity due to reduced percolation pathways [58]. While these phenomena could potentially explain the trends at higher temperatures, FTIR and XRD measurements indicate that the films in this work are primarily amorphous. This suggests that other factors, such as mechanical strain [59] or nitrogen coordination [60], may differ at higher temperatures, such that a balancing effect on transmittance, optical constants, and conductivity is observed, despite the increase in oxynitride bonding. This demonstrates the complexity of the interrelated effects of deposition temperature, precursor decomposition, purge time and efficiency, and secondary reactions responsible for the oxynitride formation.

Lastly, the ALD minimum temperature for this process based on the GPC vs. temperature plot is found at 200°C[49]. However, at least in terms of minimum carbon content, 275°C seems to be the optimal temperature. At this temperature though, the films are significantly more absorbing and conducting. This observation, while underscoring the complex nature of the ALD chemistry involved, also highlights the ability to tune the film properties within a specific range using the deposition conditions.

## Conclusions:

This study investigates the properties of $TiO_2$ films grown by atomic layer deposition (ALD) using tetrakis(dimethyl amino)titanium (IV) (TDMAT) and $H_2O$ at temperatures between 150°C – 350°C with 5s, 10s, and 30s purge times. We find that increasing the process temperature leads to increased incorporation of oxynitride bonds that affect the film's optical and electrical properties. Based on consistent results between the various measurement techniques, UV-Vis and SE measurements may serve as reliable indicators of oxynitride impurities in the bulk of the films. Overall, these results demonstrate the presence of secondary ALD reaction pathways that may lead to significant variation of the film properties across process conditions. However, these variations are relatively well-controlled and very reproducible, providing a pathway to tailor the film properties via the deposition process.


## Acknowledgments

We would like to thank Dr. Ilkeun Lee from the University of California, Riverside (UCR) for the XPS measurements and Dr. Tanguy Terlier from Rice University for the ToF-SIMS measurements. We thank Andrea Donohue from Woollam for her assistance with the optical models. We are grateful to Dr. Lisa Kelly and her students from the Department of Chemistry and Biochemistry at UMBC for their assistance with obtaining the transmission data. We kindly acknowledge Dr. Karen Gaskell and Dr. Peter Zavalij from the University of Maryland, College Park (UMD) for their help in obtaining AFM and XRD data. We also acknowledge the support of the Maryland NanoCenter and its FabLab.

## Funding

Student support is provided by an NIGMS Graduate Research Training Initiative for Student Enhancement (G-RISE) Grant (T32-GM144876). This material is based upon work supported by the National Science Foundation (NSF) under grant DMR-1905305.


# References


[1] F. Zhang, S. Yang, Y. Du, C. Li, J. Bao, P. He, H. Zhou, *Chem. Commun.* **2020**, *56*, 6396.
[2] E. C. Okpara, O. C. Olatunde, O. B. Wojuola, D. C. Onwudiwe, *Environ. Adv.* **2023**, *11*, 100341.
[3] J.-P. Niemelä, G. Marin, M. Karppinen, *Semicond. Sci. Technol.* **2017**, *32*, 093005.
[4] S. A. Ansari, M. M. Khan, M. O. Ansari, M. H. Cho, *New J. Chem.* **2016**, *40*, 3000.
[5] Z. Essalhi, B. Hartiti, A. Lfakir, M. Siadat, in *2010 Int. Conf. Electron. Devices Syst. Appl.*, IEEE, Kuala Lumpur, Malaysia, **2010**, pp. 365–367.
[6] A. Khlyustova, N. Sirotkin, T. Kusova, A. Kraev, V. Titov, A. Agafonov, *Mater. Adv.* **2020**, *1*, 1193.
[7] D. Saha, R. S. Ajimsha, K. Rajiv, C. Mukherjee, M. Gupta, P. Misra, L. M. Kukreja, *Appl. Surf. Sci.* **2014**, *315*, 116.
[8] X. Li, X. Li, B. Zhu, J. Wang, H. Lan, X. Chen, *RSC Adv.* **2017**, *7*, 30956.
[9] M. Bowker, C. O'Rourke, A. Mills, *Top. Curr. Chem.* **2022**, *380*, 17.
[10] T. S. Natarajan, V. Mozhiarasi, R. J. Tayade, *Photochem* **2021**, *1*, 371.
[11] Q. Chen, A. Ozkan, B. Chattopadhyay, K. Baert, C. Poleunis, A. Tromont, R. Snyders, A. Delcorte, H. Terryn, M.-P. Delplancke-Ogletree, Y. H. Geerts, F. Reniers, *Langmuir* **2019**, *35*, 7161.
[12] H. Xiong, L. Wu, Y. Liu, T. Gao, K. Li, Y. Long, R. Zhang, L. Zhang, Z. Qiao, Q. Huo, X. Ge, S. Song, H. Zhang, *Adv. Energy Mater.* **2019**, *9*, 1901634.
[13] K. J. Ramos-Corella, M. Sotelo-Lerma, A. A. Gil-Salido, J. L. Rubio-Pino, O. Auciello, M. A. Quevedo-López, *Mater. Technol.* **2019**, *34*, 455.

[14] J. Aarik, A. Aidla, H. Mändar, T. Uustare, *Appl. Surf. Sci.* **2001**, *172*, 148.
[15] R. Hussin, K. L. Choy, X. Hou, *SSN* **2016**, *11*.
[16] B. Abendroth, T. Moebus, S. Rentrop, R. Strohmeyer, M. Vinnichenko, T. Weling, H. Stöcker, D. C. Meyer, *Thin Solid Films* **2013**, *545*, 176.
[17] R. Kuis, T. Gougousi, I. Basaldua, P. Burkins, J. A. Kropp, A. M. Johnson, *ACS Photonics* **2019**, *6*, 2966.
[18] R. W. Johnson, A. Hultqvist, S. F. Bent, *Mater. Today* **2014**, *17*, 236.
[19] J. C. Hackley, T. Gougousi, *Thin Solid Films* **2009**, *517*, 6576.
[20] M. Ylilammi, *Thin Solid Films* **1996**, *279*, 124.
[21] J. S. Becker, E. Kim, R. G. Gordon, *Chem. Mater.* **2004**, *16*, 3497.
[22] D. M. Hausmann, R. G. Gordon, *J. Cryst. Growth* **2003**, *249*, 251.
[23] D. Nečas, P. Klapetek, *Cent. Eur. J. Phys.* **2012**, *10*, 181.
[24] J. N. Hilfiker, N. Singh, T. Tiwald, D. Convey, S. M. Smith, J. H. Baker, H. G. Tompkins, *Thin Solid Films* **2008**, *516*, 7979.
[25] J. N. Hilfiker, M. R. Linford, *Vac. Technol. Coat.* **2022**, *23*, 33.
[26] R. A. Synowicki, *Phys. Status Solidi C* **2008**, *5*, 1085.
[27] J. A. Woollam Co., Inc., **2011**.
[28] H.-Q. Jiang, Q. Wei, Q.-X. Cao, X. Yao, *Ceram. Int.* **2008**, *34*, 1039.
[29] J. N. Hilfiker, M. R. Linford, *Vac. Technol. Coat.* **2022**, *23*, 28.
[30] W.-J. Lee, E.-Y. Yun, H.-B.-R. Lee, S. W. Hong, S.-H. Kwon, *Data Brief* **2020**, *31*, 105777.
[31] H. Jain, P. Poodt, *Dalton Trans.* **2021**, *50*, 5807.
[32] R. Methaapanon, S. F. Bent, *J. Phys. Chem. C* **2010**, *114*, 10498.
[33] H. Zhang, B. Wang, B. Brown, *Appl. Surf. Sci.* **2020**, *521*, 146349.
[34] T. Kato, Y. Yamada, Y. Nishikawa, T. Otomo, H. Sato, S. Sato, *J. Mater. Sci.* **2021**, *56*, 15798.
[35] R. Quesada-Cabrera, C. Sotelo-Vazquez, J. A. Darr, I. P. Parkin, *Appl. Catal. B Environ.* **2014**, *160–161*, 582.
[36] L. Braic, N. Vasilantonakis, A. Mihai, I. J. Villar Garcia, S. Fearn, B. Zou, N. McN. Alford, B. Doiron, R. F. Oulton, S. A. Maier, A. V. Zayats, P. K. Petrov, *ACS Appl. Mater. Interfaces* **2017**, *9*, 29857.
[37] X. Song, D. Gopireddy, C. G. Takoudis, *Thin Solid Films* **2008**, *516*, 6330.
[38] M. V. Kuznetsov, Ju. F. Zhuravlev, V. A. Zhilyaev, V. A. Gubanov, *J. Electron Spectrosc. Relat. Phenom.* **1992**, *58*, 1.
[39] A. G. Shard, *J. Vac. Sci. Technol. A* **2020**, *38*, 041201.
[40] W. J. Maeng, S.-J. Park, H. Kim, *J. Vac. Sci. Technol. B Microelectron. Nanometer Struct. Process. Meas. Phenom.* **2006**, *24*, 2276.
[41] H. G. Tompkins, *J. Appl. Phys.* **1991**, *70*, 3876.
[42] Z. Wang, L. Lai, T. Zhang, S. Wu, J. Zhao, Y. Zhao, Y. Jin, J. Wang, S. Fan, Q. Li, *ACS Appl. Energy Mater.* **2021**, *4*, 10542.
[43] Z. N. Jameel, A. J. Haider, S. Y. Taha, *Eng. Technol. J.* **2014**, *32*, 418.
[44] Waltman, R, Kellock, A, *J. Vac. Sci. Technol. Vac. Surf. Films* **2003**.
[45] A. Jolivet, C. Labbé, C. Frilay, O. Debieu, P. Marie, B. Horcholle, F. Lemarié, X. Portier, C. Grygiel, S. Duprey, W. Jadwisienczak, D. Ingram, M. Upadhyay, A. David, A. Fouchet, U. Lüders, J. Cardin, *Appl. Surf. Sci.* **2023**, *608*, 155214.
[46] L. Yu. Beliaev, E. Shkondin, A. V. Lavrinenko, O. Takayama, *Opt. Mater.* **2023**, *143*, 114237.
[47] D. Hiller, F. Munnik, J. López-Vidrier, D. Solonenko, J. Reif, M. Knaut, O. Thimm, N. E. Grant, *J. Vac. Sci. Technol. A* **2024**, *42*, 032406.
[48] J. L. Vazquez-Arce, T. Suta, B. Fodor, L. Makai, O. Contreras, A. Bahrami, K. Nielsch, H. Tiznado, *Adv. Mater. Interfaces* **2024**, 2400269.

[49] E. V. Skopin, K. Abdukayumov, P. Abi Younes, M. Anikin, H. Roussel, J.-L. Deschanvres, H. Renevier, *Thin Solid Films* **2021**, *723*, 138591.
[50] C. G. Granqvist, A. Hultåker, *Thin Solid Films* **2002**, *411*, 1.
[51] Z. Y. Banyamin, P. J. Kelly, G. West, J. Boardman, *Coatings* **2014**, *4*, 732.
[52] Y. G. Khim, B. Park, J. E. Heo, Y. H. Khim, Y. R. Khim, M. Gu, T. G. Rhee, S. H. Chang, M. Han, Y. J. Chang, *J. Korean Phys. Soc.* **2023**, *82*, 486.
[53] E.-J. Song, H. Jo, S.-H. Kwon, J.-H. Ahn, J.-D. Kwon, *Thin Solid Films* **2020**, *694*, 137752.
[54] B. Xia, J.-J. Ganem, I. Vickridge, E. Briand, S. Steydli, R. Benbalagh, F. Rochet, *Appl. Surf. Sci.* **2022**, *601*, 154233.
[55] L. Ye, J. A. Kropp, T. Gougousi, *Appl. Surf. Sci.* **2017**, *422*, 666.
[56] J. P. A. M. Driessen, J. Schoonman, K. F. Jensen, *J. Electrochem. Soc.* **2001**, *148*, G178.
[57] Z. Lei, *Trans Nonferrous Met SOCChina* **2007**.
[58] T. Ryll, A. Brunner, S. Ellenbroek, A. Bieberle-Hutter, J. L. M. Rupp, L. J. Gauckler, *Phys. Chem. Chem. Phys.* **2010**, *12*, 13933.
[59] H.-F. Lee, S. Kumar, M. A. Haque, *Acta Mater.* **2010**, *58*, 6619.
[60] X. Li, C. Wang, H. Xue, H. Pang, Q. Xu, *Coord. Chem. Rev.* **2020**, *422*, 213468.